The Effect of Gum Arabic Addition on Lignosulfonate/ Polyvinyl Alcohol Composite Films

Emir Erişir

The effectiveness of Gum Arabic (GA) as a compatibilizer was evaluated in sodium lignosulfonate (LS)/polyvinyl alcohol (PVOH) composite film systems. This study aimed to improve the morphological integrity and mechanical stability of films, while achieving sustainability objectives. The goal was to obtain mechanically reinforced and morphologically homogeneous biodegradable films through GA-assisted phase stabilization. The structural, morphological, and mechanical properties, as well as the water interaction performance, of films were investigated. Fourier transform infrared analysis showed that the band intensity attributed to hydrogen bonding increased with the addition of GA, indicating enhanced molecular interactions. Scanning electron microscopy revealed that GA increased morphological defects such as microphase separation and aggregation, especially at low concentrations. While 25% GA helped fill the pores, it did not completely eliminate structural defects. Mechanical tests showed a decrease in tensile strength of up to 63% associated with such defects. Water sorption and dissolution tests showed that mass loss in aqueous media reached 75% due to the solubility of LS and GA. However, higher GA content moderately reduced this loss by minimizing defect sites. GA failed to act as a compatibilizer under tested formulation and processing parameters but contributed to the film's surface homogeneity as a physical filler.

DOI: 10.15376/biores.21.2.3688-3717

Keywords: Gum arabic; Sodium lignosulfonate; Polyvinyl alcohol; Biodegradable polymers; Film production

Contact information: Department of Paper Technology, Sakarya University of Applied Sciences, Esentepe Kampüsü T4 Binası – SAYEM Sakarya, Turkiye; Email: emirerisir@subu.edu.tr

INTRODUCTION

With increasing awareness of sustainability, petroleum-based materials are losing their market share. Especially, because of their low biodegradability, this shift is being pushed along by various laws. For example, the European Union recently launched a Circular Economy Action Plan. According to the plan, new regulations regarding single-use plastics will be introduced by 2030 and 2040, limiting the use of these types of plastics and to use a certain percentage of recycled materials in their production. As a result, the reduction of certain plastics is expected to increase interest in natural polymers such as cellulose, starch, and lignin.

It is estimated that plants produce between 150 to 180 billion tons of biomass each year, with around 20% of that being lignin (Kropat *et al.* 2021). Approximately 20 billion tons of lignin are synthesized annually, and the total mass of lignin in the biosphere is around 300 billion tons (Gonçalves *et al.* 2021). This enormous amount makes it the second

most abundant biopolymer in nature after cellulose (Su and Fang 2014; Fuentalba *et al.* 2025).

The bulk of lignin generated in industries is produced by the separation of polysaccharides from the biomass during the processes employed in the pulping industries. During the pulping process, annually 50 to 70 billion kg of lignin and its derivatives are produced (Hu *et al.* 2018). Current processes result in approximately 95% of produced lignin being burned for energy generation and chemical recovery (Grossman and Vermerris 2019), a method reported to yield about $80 USD per ton (Luo and Abu-Omar 2017). It is clear that this valuable by-product has not received sufficient attention. However, a forecast on the development of the global lignin market predicts that its market size could reach US $1.12 billion by 2027 (Kropat *et al.* 2021).

Lignosulfonate (LS) is the most commercially available type of lignin. It is used in diverse areas, from the construction industry to agricultural applications and differs from kraft, soda, and organosolv lignin in its molecular structure and properties (Kropat *et al.* 2021). Changing the molecular structure and properties increases its potential value and applicability (Lin *et al.* 2014). However, LS, like other types of natural lignin, has certain limitations. To increase its versatility, modification techniques are applied, or it is combined with other substances that can complement its deficiencies.

Polyvinyl alcohol (PVOH), a semi-synthetic material, is an alternative for matrix production due to its low toxicity and biodegradability. Its high film-forming ability, satisfactory mechanical properties, transparency, and biocompatibility contribute to its importance in various applications (Korbag *et al.* 2018). Due to the strong hydrogen bonding network facilitated by its hydroxyl groups (Li *et al.* 2022), it is utilized in a variety of applications, ranging from packaging materials to wound dressings and even in the production of graphene. Nonetheless, its affinity for water complicates its application in environments where moisture is prevalent (Zhang *et al.* 2020). Consequently, it finds application in combinations with different natural polymers.

Lignin is preferred for PVOH matrices in composite production due to its biocompatibility, biodegradability, thermal stability, and UV-shielding properties (Ramadhan *et al.* 2024). The studies using various types of lignin as additives for the production of PVOH films provide examples. These studies have shown improvements in both the mechanical and barrier properties of lignin (Phansamarng *et al.* 2024; Ramadhan *et al.* 2024). There are also studies that establish a relationship between lignin content and the thermal properties of PVOH composites (Xu *et al.* 2023). The observed increase in the performance properties of LS/PVOH matrices is generally attributed to the strong intramolecular and intermolecular hydrogen bonds between the polymers and the abundance of OH groups, which provide effective interfacial adhesion (Nair *et al.* 2014). However, 5% is considered the critical concentration limit for lignin concentration in the lignin/PVOH matrix. Using higher concentration, aggregate formation occurs being negative impact on mechanical performance properties (Ye *et al.* 2016, Zhang *et al.* 2020). To increase the lignin concentration in LS/PVOH matrices, it is necessary to improve the compatibility between polymers and prevent the formation of polymer aggregates, and the additives are used for this purpose.

Gum Arabic (GA), with a complex chemical structure, is an important natural-based polysaccharide. Its main chain consists of β-D-galactopyranosyl units interconnected by 1,3-linkages, and side branches containing functional groups such as L-arabinose, L-rhamnose, and D-glucuronic acid. Its solubility in water has led to its utilization in various

fields including food, medicine, hydrogels, biomaterials, cosmetics, textiles, paper, ink, printing, paint, and adhesives (Patel and Goyal 2015; Rostamabadi *et al.* 2024).

GA is also used for film production and as an emulsifying agent. Both of these properties help distribute polymer phases evenly in mixed biopolymer systems, even when GA is used in small amounts (Rostamabadi *et al.* 2024). However, the films made only from GA tend to be brittle, which limits their use and processing without other polymers such as polylactic acid to create films that are mechanically stronger and more stable (Onyari *et al.* 2008). Beyond its structural function, numerous investigations have revealed GA's ability to interact with lignin via substantial hydrogen bonding, and under specific circumstances, it may even establish partial covalent bonds (Gorish *et al.* 2025). Furthermore, GA has been employed to facilitate a more uniform polymer distribution within nanocellulose-reinforced starch film matrices, leading to reduced vapor permeability and increased tensile strength (Vigneshwaran *et al.* 2011).

Numerous comprehensive studies have been conducted on the LS/PVOH, GA/PVOH and GA/LS binary systems. However, it has not yet been determined how GA will function within the LS/PVOH system. In this study, it was hypothesized that GA may create the homogeneous dispersion of polymers in the LS/PVOH system and thereby yield uniform films with improved mechanical strength. The primary objective of this study was to reduce or eliminate the effects of phase separation problems arising from the use of high concentrations of LS in LS/PVOH films. To determine these effects, several analytical test methods were applied to the parent polymers and the resulting films, and the results were evaluated comparatively.

EXPERIMENTAL

Materials

Sodium lignosulfonate (LS, Sigma Aldrich, CAS No: 8061-51-6, M_w: ~52000 g/mol, M_n: ~7000), polyvinyl alcohol (PVOH, Merck, ≥ 98% hydrolyzed, M_w: 60000 g/mol), Gum Arabic (GA, kordofan Gum Arabic, CAS No: 9000-01-5, food grade, purity ≥ 98%), glycerol (Balmumcu Kimya, USP grade, M_w: 92.09 g/mol), and urea (Merck, M_w: 60.06 g/mol, purity ≥ 99%) were procured and utilized without further purification. Deionized (DI) water was used in all production and characterization steps.

Production of LS-PVOH-GA Films

In this study, a final weight for each film was set at 2.00 g. The composite film matrix ultimately consists of a mixture of 1.00 g of GA (a%) and PVOH (100% – a%) with 1.00 g of LS. The proportions of PVOH, a semi-synthetic polymer, and GA, a natural polysaccharide, were methodically adjusted (0, 1, 5, 10, or 25%). During the preparation of the film solutions, calculations were made for the production of two films.

The evaporation time of the solvent was considered an essential factor in the formulation of the film solutions. To investigate the potential effect of this stage on film morphology and thus the final properties, two different pre-evaporation times, 60 and 90 min, were applied. Through extending the evaporation time, it was expected that the total solid concentration in the solution would increase, which would, in turn, affect the interactions between the polymers and phase separation. This approach made it possible to better understand the dynamics of the film formation process and to determine the role of

this parameter in the formation of structural defects. Film production was carried out using the processes described below:

1. *The preparation of the PVOH solution:* To achieve a final polymer matrix weight of 2.00 g, PVOH at the concentration defined above was dissolved in 20 mL of DI water in an oil bath operating at 85 to 90 °C under continuous magnetic stirring at a constant speed of 500 rpm.
2. *The preparation of LS-GA solution:* The specified amount of GA, determined according to its desired percentage (0, 1, 5, 10, 25% based on PVOH amount) in the total polymer matrix of 2.00 g, was combined with around 2.00 g of LS, 0.20 g of urea, and 4.00 mL of a 25 wt% glycerol solution. This mixture was then dissolved in 20 mL of deionized water at room temperature at a constant speed of 500 rpm and heated after completed dissolution.
3. *The preparation of the final film formation solution:* After preparing the LS-GA and PVOH solutions separately, these solutions were combined in the same reaction vessel. The reaction vessel lid was closed and stirred for 60 min using a magnetic stirrer at 500 rpm to obtain a homogeneous final solution. The reaction vessel was kept in an oil bath at 85 to 90 °C.
4. *Pre-evaporation process:* To increase the concentration of the film solution, the lid was opened to allow some solvent (DI water) to evaporate. Pre-evaporation was performed for 60 or 90 min.
5. *Film casting and storage:* The film-forming solution was carefully poured into two silicone molds with an inner diameter of 100 mm and left to dry in a controlled environment at 28 °C for 12 to 16 h in a climate-controlled environment.

At the end of the drying process, the films were carefully removed from the molds and securely placed in zippered plastic bags for storage.

Methods

The lignin and ash content of LS were determined using TAPPI T222 om-11 (2011) and TAPPI T211 om-02 (2002) standards, respectively. The other methods and equipment used in the study are described below.

Analytical methods

The instrumental analyses included Nuclear Magnetic Resonance (^{13}C-NMR), Fourier Transform Infrared Spectroscopy (FTIR), tensile testing, and Scanning Electron Microscopy (SEM). ^{13}C-NMR analysis was conducted to identify the structure of LS using a Bruker Ascend 500 MHz spectrometer, with DMSO-d_6 as solvent at a working concentration of 20 g/L. The FTIR spectra were recorded with a Bruker Alpha I instrument for the structural characterization of films and neat polymers. Measurements for films were taken at multiple points on both surfaces to confirm the layered structure. The spectra were obtained in the 4000 to 400 cm^{-1} range with a resolution of 4 cm^{-1}. Tensile testing was performed with an Instron Model 3345 to determine film strength. Film samples (90 × 10 mm^2) with thicknesses of 1.226 to 1.567 mm (Table S1) were tested at a speed of 20 mm/min and a maximum load of 5 kN. Each test was performed in triplicate. The SEM imaging (Thermo Scientific Asia) was employed to examine film morphology. Images were taken from both the open (exposed) and closed (mold-contact) surfaces. Samples were coated with gold–palladium and imaged at magnifications of 100×, 1000×, 2500×, and 5000×, under 15 kV accelerating voltage and vacuum.

Water absorption and dissolution

The samples (10 x 10 mm^2) were subjected to the immersion method to determine water absorption and dissolution in the films. Prior to the tests, the samples were dehydrated in an oven at 60 °C for 24 h until a stable weight was attained. This procedure guarantees full removal of all moisture from the samples. The dry samples were immersed in water at the room temperature. After determining the initial dry weights of the samples, measurements were repeated at 1, 2, 3, 6, 24, 48, and 72 h. The percentage (%) of water absorption of the samples was calculated using the weight measurements. The percentage of water absorption (%WA) was determined using Eq. 1,

$$WA\% = (W_2\text{-}W_1) \times 100 / W_1 \quad (1)$$

where W_1 represents the oven-dried weight (g) of the sample, and W_2 represents the weight (g) of the sample subsequent to immersion in water.

At the end of the 72-h water immersion period, the samples were removed and dried to determine their final mass. To determine the amount of dissolved material, the containers used in the water immersion experiments were dried at 40 °C until completely dry, and residual material was calculated.

RESULTS AND DISCUSSION

Structural Characterization of Na-Lignosulfonate

Wet analyses showed the LS was composed of 94.6% lignin and 7.26% ash. ^{13}C-NMR spectrum (Fig. S1 in Appendix) showed no distinct signals in the 90 to 102 ppm range (Yang *et al.* 2017), indicating high purity with minimal polysaccharide content. Both results allow focusing on lignin-based interactions. A resonance of dimethyl sulfoxide-d6 (DMSO-d_6), used as a solvent, was detected in the 39.5 ppm band, confirming that the sample was effectively dissolved. The signals observed in the range of 112.2 to 159.0 ppm clearly reveal the aromatic structure of lignin (Xia *et al.* 2001; Korbag and Saleh 2016; Phansamarng *et al.* 2024). The major signal at 158.5 ppm corresponds to the C-4 atom in the p-coumaric acid ester framework (Yang *et al.* 2017), while C-5 aromatic C-H bonds were observed at 115.6 ppm (Nasef *et al.* 2024). However, signals observed at 112.2 and 119.1 ppm, respectively, correspond to the C-2 and C-6 aromatic C-H bonds (Nasef *et al.* 2024) in the same region, exhibit a lower intensity compared to the previous signals. The absence of signals for aliphatic oxygen-containing groups (C-O) or methoxy (-OCH_3) groups indicates that these functional groups were below the detectable levels in the stock lignin or may have previously modified.

Fourier Transform Infrared Spectroscopy (FTIR) Analysis

The FTIR spectra from both film surfaces and neat polymers were analyzed to assess structural characteristics. In Fig. 1, the spectra for explaining these interactions are displayed separately.

Characteristic properties of neat polymers

The bands showing the characteristic vibrations determined for each polymer are presented in Fig. S2 in the Appendix. The PVOH showed a strong and broad band between 3000 to 3700 cm^{-1}, which is linked to O–H stretching vibrations resulting from both intramolecular and intermolecular hydrogen bonds (Bhargav *et al.* 2007). A distinct peak

at 1142 cm^{-1} is attributed to crystalline PVOH (Su and Fang 2014). Another notable signal appears in the 1700 to 1750 cm^{-1} range, indicating C=O stretching vibration. Furthermore, there were two distinct signals at 839 and 912 cm^{-1} corresponding to C=C bonds (Phansamarng *et al.* 2024).

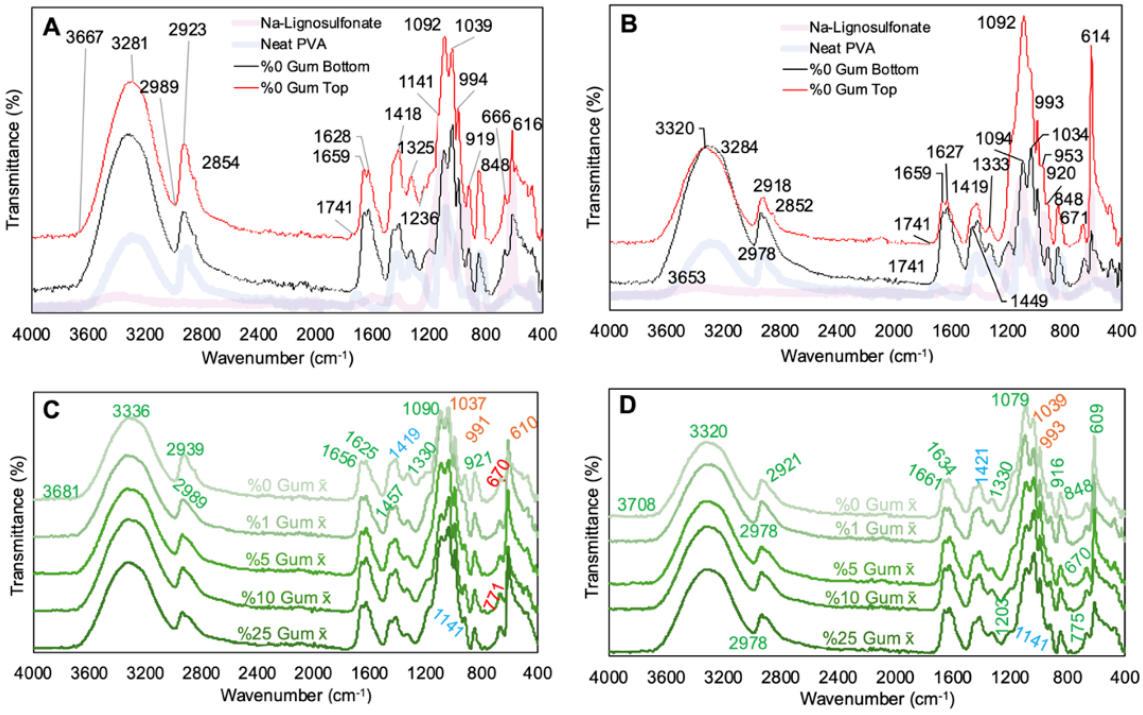

Fig. 1. FTIR spectra of films without GA are illustrated in A (60 min) and B (90 min), while spectra of GA-containing films are given in C (60 min) and D (90 min). In A and B, spectra were recorded from both surfaces of the films, with the bottom surface represented in black and the top surface in red. For GA-containing films (C and D), mean spectra were generated by averaging measurements from the top and bottom surfaces.

GA exhibited typical glycosidic C–O–C stretching at 1021 cm^{-1}, carbonyl-related bands at 1415 to 1600 cm^{-1}, and a weak O–H/C–H stretching region between 3600 and 2800 cm^{-1} (Vigneshwaran *et al.* 2011; Mudgil *et al.* 2012; Pereira *et al.* 2021; Thombare *et al.* 2023; Gorish *et al.* 2025).

The LS showed sulfonic ($-SO_3^-$) signals at 618 and 1048 cm^{-1} (Abdelrahman *et al.* 2024) and aromatic bands at 1105, 1433, and 1590 cm^{-1} (Klapiszewski *et al.* 2016; Ou and Zhao 2017; Ysulat *et al.* 2023). The hypothesis that this value is largely due to the presence of Na^+ ions (Tables S1 and 2 in Appendix) is supported by the vibrations observed at 488 cm^{-1}, which are attributed to these ions in the literature (Abdelghany *et al.* 2014).

Interactions and morphological consequences of polymers

It was confirmed by the spectra that strong physical interactions (H-bonds, van der Waals, electrostatic, hydrophobic) between PVOH and LS (Ye *et al.* 2016; Kazzaz and Fatehi 2020; Zhang *et al.* 2020; Nouh *et al.* 2023) play a crucial role for films, not chemical bonds. These interactions may result in alterations in the spectra. The broad -OH band suggested an intensified hydrogen-bonding network (Ye *et al.* 2016), consistent with physical cross-linking between LS and PVOH phases (Zhang *et al.* 2020).

The casting process revealed noticeable phase separation, pointing to limited integration of the components. In the films without GA, the C=O signal at 1741 cm^{-1} for PVOH was distinct on the top surface but nearly absent on the bottom, a result attributed to lignin aggregation and poor miscibility (Zhang *et al.* 2020; Zhou *et al.* 2022), as further confirmed by SEM. On the top surfaces, a clear band broadening was observed in the spectral region associated with LS, pointing a higher concentration of lignin.

Extending the pre-evaporation time led to a clearer phase separation. This observation highlights that the degree of separation is shaped by the specific process variables. The greater signal intensity at 610 to 620 cm^{-1} on top surfaces and the appearance of a PVOH-specific C-C stretch at 1230 to 1240 cm^{-1} (Bhargav *et al.* 2007) on bottom surfaces validated an LS-rich upper structure and a PVOH-rich lower structure.

The addition of GA created differences in the density of C-O-C and S-O bands, indicating that LS became increasingly dominant in the film structure (Fig. 1). The addition of GA intensified the -OH band, indicating a reinforced hydrogen bond system (Gorish *et al.* 2025). The signal for GA-specific glycosidic bonds became stronger as the GA concentration was increased (from 0 to 25%), while the signal showing the semi-crystalline structure of PVOH was weakened by a reduction of its concentration.

In addition, a consistent downward shift was observed in the broad O–H stretching band (from about 3350–3370 cm^{-1} to 3310–3330 cm^{-1}) with increasing GA concentration. Similar redshift phenomena, a sign of stronger hydrogen bonding, have been observed in PVOH–lignin composites (Ye *et al.* 2016; Korbag and Saleh 2016) and PVOH–polysaccharide systems (El-Nemr *et al.* 2020; Gui *et al.* 2024). Furthermore, the C=O stretching band, located between 1700 and 1740 cm^{-1}, exhibited a slight upshift, approximately 5 to 10 cm^{-1}, which is attributed to the reorganization of carbonyl groups involved in hydrogen bonding interactions. These spectral alterations provide evidence that the incorporation of GA enhanced the hydrogen-bonding network within the LS/PVOH matrix, thereby promoting molecular association and mitigating phase heterogeneity.

Mechanical Properties of Composite Films

The mechanical properties of the films were evaluated by tensile strength (Fig. 2). A notable reduction in the mechanical properties of the films was found with higher GA concentration. Increasing polysaccharide content while diminishing PVOH concentration resulted in a reduction of tensile strength by as much as 63%.

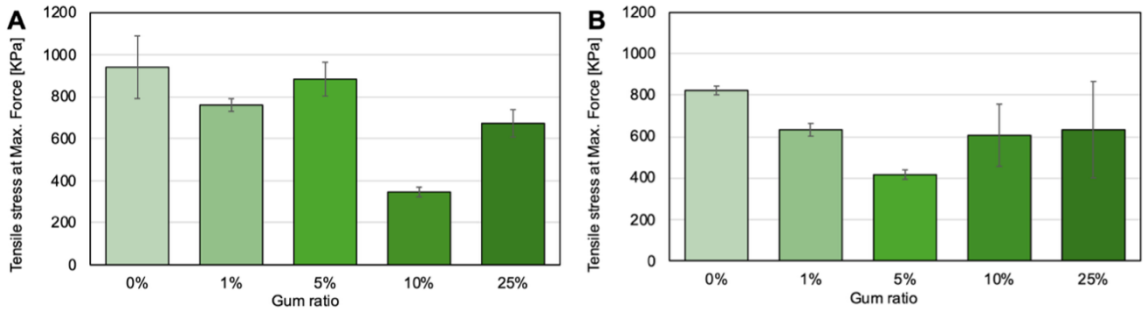

Fig. 2. The effect of GA concentration on tensile strength in LS/PVOH films (A for 60 min and B for 90 min)

Research demonstrates that elevating the LS concentration to an optimal level (Ye *et al.* 2016; Zhang *et al.* 2020; Li *et al.* 2022; Baite *et al.* 2023; Xu *et al.* 2023; Phansamarng

et al. 2024; Ramadhan *et al.* 2024) enhances tensile strength *via* mechanisms including hydrogen bond formation, the rigidity of lignin, and superior interfacial adhesion.

However, the use of high LS concentrations has been shown to lead to lower tensile strength values. It is thought that as LS concentration increases, the dispersion bonding percentage increases (Ramadhan *et al.* 2024), interfacial adhesion decreases (Phansamarng *et al.* 2024), and lignin particles aggregate within the PVOH matrix, leading to microphase separation (Yang *et al.* 2024). As a result of this assumption, irregular LS-PVOH bonds are thought to occur, causing lignin to act solely as a filler. The results of Xu *et al.* (2013) are similar, and they found similar reductions in mechanical properties.

Scanning Electron Microscope

As shown in the SEM images (Figs. 3 through 7), changes in GA content (0 to 25%) together with differences in pre-evaporation time (60 or 90 min) altered the morphology of the films. Variations were also evident in porosity and surface roughness. The control sample (0% GA) showed a heterogeneous structure with phase separation and polymer aggregates due to poor LS/PVOH compatibility (Kubo and Kadla 2003; Wang *et al.* 2020), corroborated by FTIR findings.

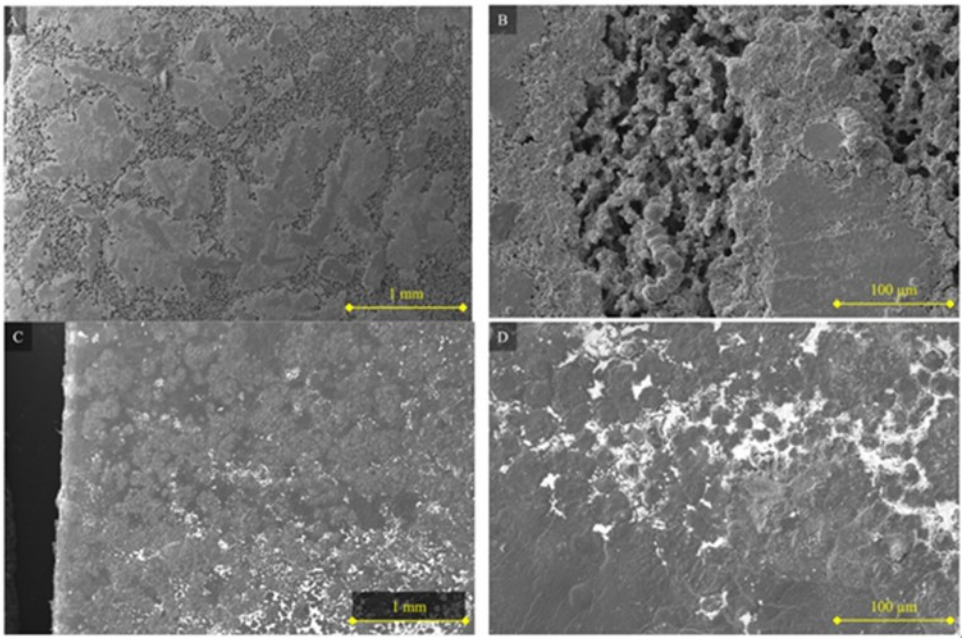

Fig. 3. Electron microscope images of the films without gum addition are shown after 60 min of pre-evaporation. The bottom surface is shown in A at 100× and in B at 1000× magnifications. The top surface is displayed in C at 100× and in D at 1000× magnifications.

Even low GA concentrations (1% and 5%) increased morphological defects (Figs. 4 and 5) leading to greater porosity. The structural changes became more apparent by the concentration of GA to 10%. This was shown by the appearance of distinct micro-pores and polymer aggregates, which were visible on a millimeter scale (Fig. 6). These morphological defects are also the main reason for the decrease in the mechanical strength of the films.

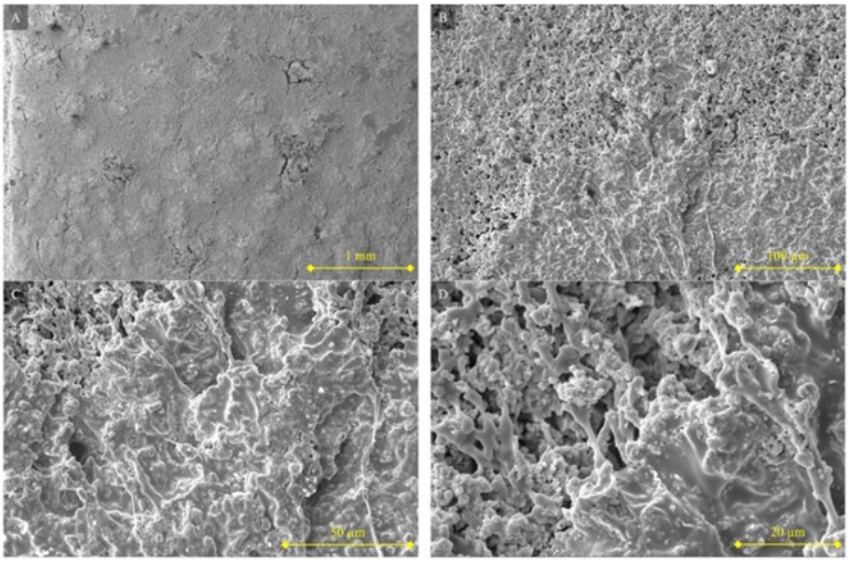

Fig. 4. Electron microscope images of films with 1% gum addition after 60 min of pre-evaporation are presented. The bottom surface is shown in A at 100× and in B at 1000× magnifications. The top surface is displayed in C at 2500× and in D at 5000× magnifications.

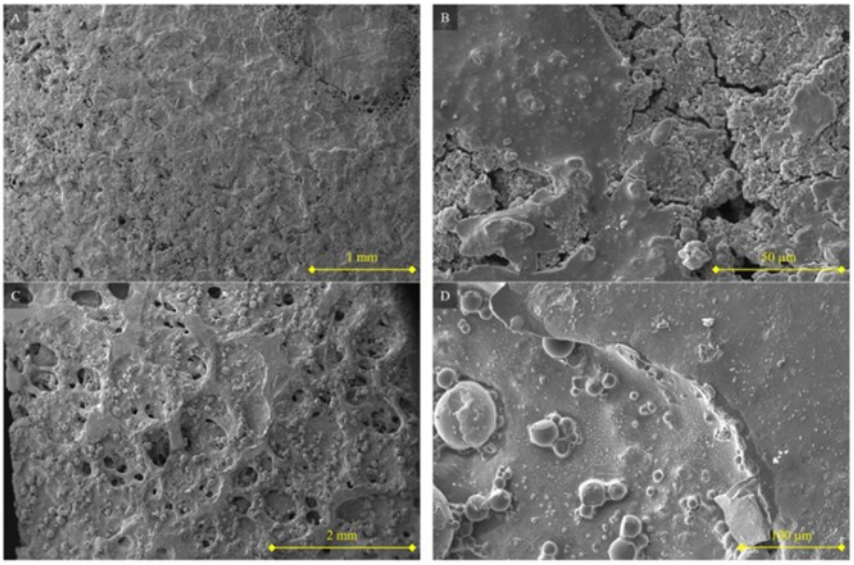

Fig. 5. Electron microscope images of films with 5% gum addition after 60 min of pre-evaporation are presented. The bottom surface is shown in A at 100× and in B at 2500× magnifications. The top surface is displayed in C at 70× and in D at 1000× magnifications.

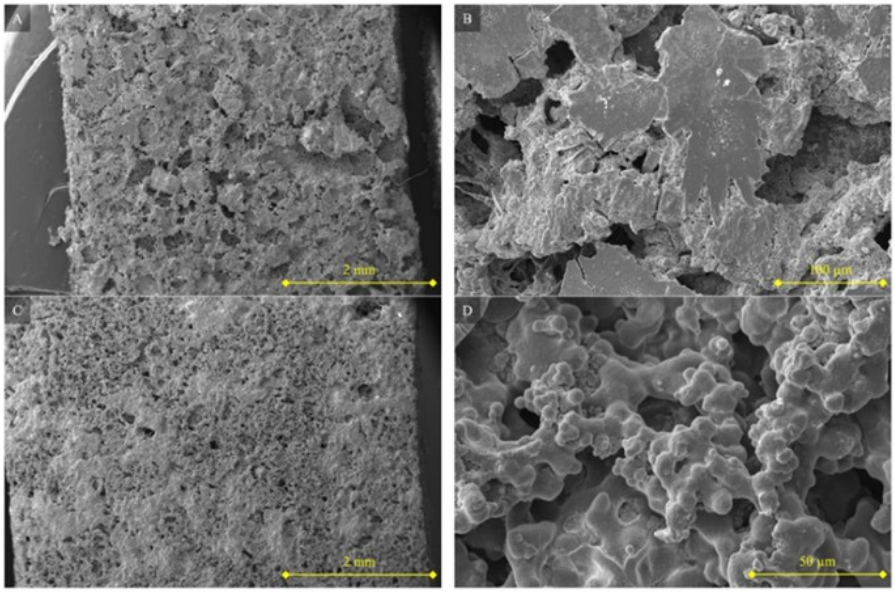

Fig. 6. Electron microscope images of films with 10% gum addition after 60 min of pre-evaporation are presented. The bottom surface is shown in A at 70× and in B at 1000× magnifications. The top surface is displayed in C at 70× and in D at 2500× magnifications.

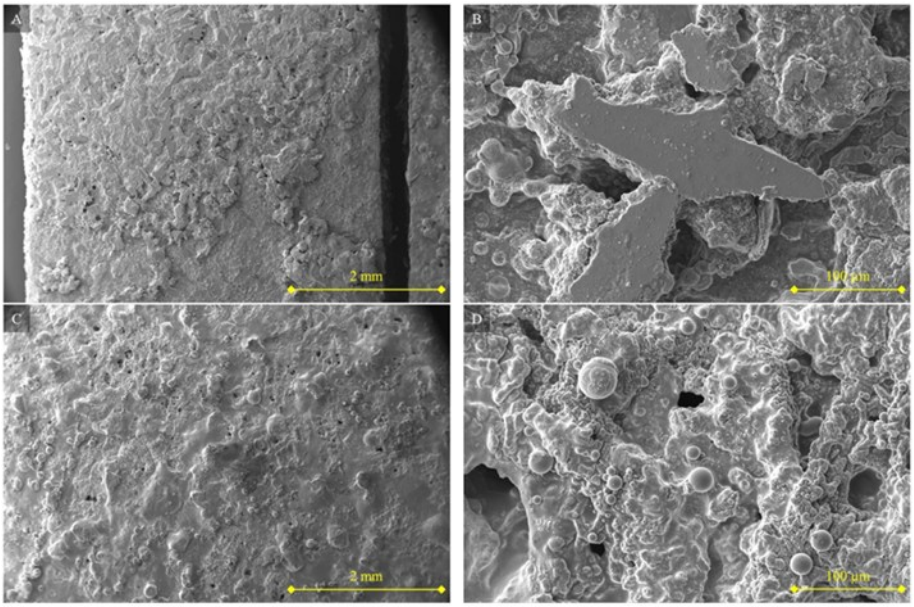

Fig. 7. Electron microscope images of films with 25% gum addition after 60 min of pre-evaporation are presented. The bottom surface is shown in A at 70× and in B at 1000× magnifications. The top surface is displayed in C at 70× and in D at 1000× magnifications.

Conversely, elevating the polysaccharide concentration to 25% yielded a favorable outcome, with GA functioning as a filler, addressing morphological defects and pores (Fig. 7A, C, and D). Nonetheless, the general heterogeneous structure and the creation of aggregates continued. This conclusion aligns with existing work indicating that some LS functions merely as a filler rather than forming a binding with PVOH (Xu *et al.* 2013). Extending the pre-evaporation time to 90 min results in the polymer clusters (Fig. 8B), an increase in both the quantity and dimensions of pores (Fig. 8C), and the emergence of white

patches (Fig. 8D) on the film surfaces as the gum concentration rises relative to films with 0% GA additive.

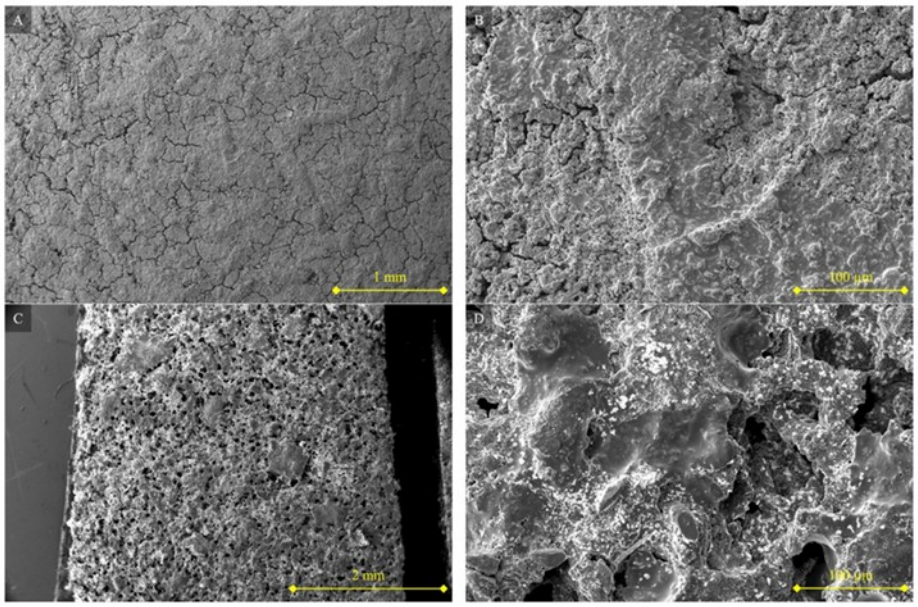

Fig. 8. SEM images of films containing 1% (A, B) and 10% (C, D) GA after 90 min pre-evaporation, shown at 70× and 1000× magnifications

Elemental mapping results (Tables S1 and S2) showed that Na^+ and $–SO_3^–$, representing the LS phase, were mainly concentrated at the film surface in 60-min pre-evaporated samples, while shifting toward the bottom in 90-min samples. This inversion indicates phase separation between LS and PVOH domains. Consistent with FTIR results, the higher oxygen content in LS-rich regions indicates that GA primarily interacts with LS. It was reported that similar compositional redistribution occurred in lignin–PVOH films under extended drying or humidity cycling conditions (Gui *et al.* 2024; Wang *et al.* 2024; Li *et al.* 2022).

The findings from Fourier-transform infrared spectroscopy (FTIR) and scanning electron microscopy (SEM) analyses indicate that the phase separation observed in LS/PVOH/GA films primarily originated from the poor miscibility of lignosulfonate (LS) within the polyvinyl alcohol (PVOH)-rich matrix. This theory is supported by the differences between the upper and lower film surfaces, as well as the absence of the C=O stretching band on the lower side. Similarly separated morphologies have been reported in other PVOH–lignin systems; in these cases, the hydrophilic PVOH tends to migrate toward the aqueous phase during solvent evaporation, whereas the less soluble aromatic lignosulfonate accumulates near the air interface (Xu *et al.* 2023; Tian *et al.* 2024; Erişir 2025). These studies indicate that the hydrophilic groups of PVOH are moved by the hydrophobic surface of lignin particles, thereby facilitating phase separation.

The addition of GA, an amphiphilic polysaccharide, led to a partial reduction in interfacial tension; however, complete separation reduction was not achieved, a result of its characteristic solubility limitations and competition for hydrogen-bonding sites. This phenomenon aligns with findings in PVOH–guar gum (Shaikh *et al.* 2022) and PVOH–tamarind gum (Rawooth *et al.* 2022) systems, where dual-phase microstructures were similarly observed at elevated gum concentrations. Consequently, the phase separation observed in this study indicates a thermodynamic incompatibility between LS and the

PVOH/GA matrix, a condition that is exacerbated under prolonged pre-evaporation conditions.

Water Absorption and Dissolution

All samples reached water absorption equilibrium within the first hour (Fig. 9). The control group absorbed 76.1% water. Absorption increased to 85.4% with 1% GA but decreased to 58.2% with 5% GA, maintaining ~75% at 10% and higher concentrations. Over time, film mass decreased due to polymer dissolution (Raj and Bajpai 2020), with dissolution rate exceeding absorption.

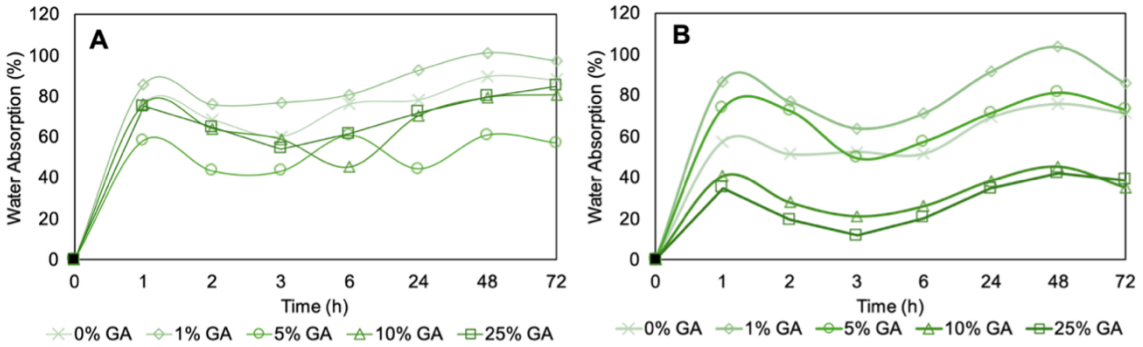

Fig. 9. The effects of GA concentration on the water absorption of LS/PVOH films are shown. Graph A presents the results for films pre-evaporated for 60 min, while Graph B displays those obtained after 90 min.

A slight drop noted around the third hour (Fig. 9/b) was not due to a measurement error. Instead, it stemmed from a brief release of moisture and internal reorganization within the LS-, PVOH-, and GA-rich domains. Temporary changes in water distribution have also been observed in PVOH–lignin and other lignin-containing biopolymer systems when subjected to alternating humidity or hydrothermal conditions (Jain *et al.* 2017; Hu *et al.* 2023; Gui *et al.* 2024; Wang *et al.* 2024; Singh *et al.* 2024).

GA, LS and PVOH are polymers with high hydrophilicity (Banegas *et al.* 2013; Rahman *et al.* 2021; Li *et al.* 2022; Phansamarng *et al.* 2024), but after 72 h immersion (Fig. 10) the control group showed minimal mass loss. Despite the reduction in PVOH content within the sample, the overall weight of the films exhibited an increase with the higher GA concentration. This phenomenon can be attributed to the covering and filling effects of GA of film surfaces mentioned before.

The highest mass loss (66% to 74%) was observed in the 1% GA-added LS/PVOH matrix. This finding is consistent with the fact that films containing 1% GA had the highest water absorption values. A general decrease in water absorption performance was observed at GA concentrations higher than 1%. These results indicate that the effect of GA on film structure varies with concentration, and that there is an optimum equilibrium point.

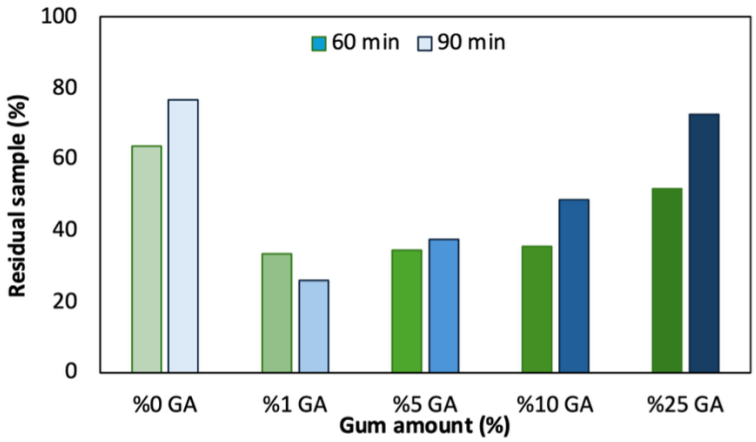

Fig. 10. The effect of GA concentration and pre-evaporation time on the residual material (%) of LS/PVOH films after 72 h of immersion in water

CONCLUSIONS

1. In contrast to the initial hypothesis, gum Arabic (GA) did not effectively interact with the lignosulfonate/poly(vinyl alcohol) (LS/PVOH) system under tested conditions. Lower GA concentrations (1% and 5%) led to microphase separation and aggregation, caused surface cracks and pores to form.
2. In the evaluated conditions, GA worked more as a filler than as a compensatory agent, especially at higher concentrations (25%).
3. The 1:1 LS/PVOH ratio used in this study was not optimal for maintaining the material's morphological stability. This composition caused phase heterogeneity and a noticeable decrease in mechanical strength. Evaluating GA performance at different LS/PVOH ratios would provide clearer insights into composition-dependent behavior.
4. GA concentration increment resulted in a decline in film strength, with tensile strength decreasing by more than 60% at higher GA levels. This reduction appears to be related to the increased aggregation tendency as the PVOH fraction decreases.
5. The concentration of GA also influenced by water absorption and dissolution in it. At lower concentrations, GA had little effect on how much water was taken up. However, higher concentrations of GA, specifically 25%, reduced mass loss. This was because GA decreased surface defects and limited water penetration. These findings were also supported by the differences in shape seen in the scanning electron microscope (SEM) images.

ACKNOWLEDGMENTS

The author gratefully acknowledges Mert Kaban (Sakarya University of Applied Sciences) for the SEM measurements and Rumeysa Yildirim (Kocaeli University) for Tensile testing measurements.

Conflict of Interest

The author declares that there is no conflict of interest regarding the publication of this manuscript. No personal, financial, or professional relationships exist that could have influenced the research or conclusions presented in this work.

REFERENCES CITED

Abdelghany, A. M., ElBatal, F. H., ElBatal, H. A., and EzzElDin, F. M. (2014). "Optical and FTIR structural studies of CoO-doped sodium borate, sodium silicate and sodium phosphate glasses and effects of gamma irradiation-a comparative study," *J. Mol. Struct.* 1074, 503-510. https://doi.org/10.1016/j.molstruc.2014.06.011

Abdelrahman, N. S., Galiwango, E., Al-Marzouqi, A. H., and Mahmoud, E. (2024). "Sodium lignosulfonate: A renewable corrosion inhibitor extracted from lignocellulosic waste," *Biomass Conv. Bioref.* 14(6), 7531-7541. https://doi.org/10.1007/s13399-022-02902-6

Baite, T. N., Purkait, M. K., and Mandal, B. (2023). "Synthesis of lignin from waste leaves and its potential application for bread packaging: A waste valorization approach," *Int. J. Biol. Macromol.* 235, article 123880. https://doi.org/10.1016/j.ijbiomac.2023.123880

Banegas, R. S., Zornio, C. F., Borges, A. D. M., Porto, L. C., and Soldi, V. (2013). "Preparation, characterization and properties of films obtained from cross-linked guar gum," *Polímeros* 23, 182-188. https://doi.org/10.4322/polimeros.2013.082

Bhargav, P. B., Mohan, V. M., Sharma, A. K., and Rao, V. N. (2007). "Structural, electrical and optical characterization of pure and doped poly (vinyl alcohol) (PVA) polymer electrolyte films," *Int. J. Polym. Mater. Polym. Biomater.* 56, 579-591. https://doi.org/10.1080/00914030600972790

El-Nemr, K. F., Mohamed, H. R., Ali, M. A., Fathy, R. M., and Dhmees, A. S. (2020). "Polyvinyl alcohol/gelatin irradiated blends filled by lignin as green filler for antimicrobial packaging materials," *J. Environ. Anal. Chem.* 100(14), 1578-1602. https://doi.org/10.1080/03067319.2019.1657108

Erişir, E. (2025). "The effects of pre-evaporation time on the structure and performance of Na-lignosulfonate/PVA composite films," *Sakarya University Journal of Science* 29(5), 580-591. https://doi.org/10.16984/saufenbilder.1750450

Fuentalba, C., Ferrer, V., Arteaga-Pérez, L. E., Santos, J., Delgado, N., Casas-Ledón, Y., Bravo-Arrepol, G., Pereira, M., Andrade, A., Escobar-Avello, D., *et al.* (2025). "Actualized scope of forestry biomass valorization in Chile: Fostering the bioeconomy," *Forests* 16(8), article 1208. https://doi.org/10.3390/f16081208

Gonçalves, S., Ferra, J., Paiva, N., Martins, J., Carvalho, L. H., and Magalhães, F. D. (2021). "Lignosulphonates as an alternative to non-renewable binders in wood-based materials," *Polymers* 13(23), article 4196. https://doi.org/10.3390/polym13234196

Gorish, B. M., Abdelmula, W. I., Dang, W., and Zhu, D. (2025). "Multifunctional lignin-gum Arabic nanocomposites: Green nanoarchitectonics via ultrasonic-assisted laccase catalysis for antimicrobial, antioxidant, and antidiabetic therapies," *Biomater. Adv.* 177, article 214390. https://doi.org/10.1016/j.bioadv.2025.214390

Grossman, A., and Vermerris, W. (2019). "Lignin-based polymers and nanomaterials," *Curr. Opin. Biotechnol.* 56, 112-120. https://doi.org/10.1016/j.copbio.2018.10.009

Gui, T., Xiao, L. P., Zou, S. L., Zhang, Y., Fu, X., Liu, C. H., and Sun, R. C. (2024). "Tough and biodegradable C-lignin cross-linked polyvinyl alcohol supramolecular composite films with closed-looping recyclability," *Chem. Eng. J*. 491, article 151748.

Hu, J., Zhang, Q., and Lee, D. J. (2018). "Kraft lignin biorefinery: A perspective," *Bioresour. Technol.* 247, 1181-1183. https://doi.org/10.1016/j.biortech.2017.08.169

Hu, Y., Luo, J., Luo, S., Fei, T., Song, M., and Qin, H. (2023). "High-strength polyvinyl alcohol-based hydrogel by vermiculite and lignocellulosic nanofibrils for electronic sensing," *e-Polymers* 23(1), article 20230081. https://doi.org/10.1515/epoly-2023-0081

Jain, N., Singh, V. K., and Chauhan, S. (2017). "A review on mechanical and water absorption properties of polyvinyl alcohol based composites/films," *J. Mech. Behav. Mater*. 26(5-6), 213-222. https://doi.org/10.1515/jmbm-2017-0027

Kazzaz, A. E., and Fatehi, P. (2020). "Interaction of synthetic and lignin-based sulfonated polymers with hydrophilic, hydrophobic, and charged self-assembled monolayers," *RSC Adv.* 10(60), 36778-36793. https://doi.org/10.1039/d0ra07554j

Klapiszewski, Ł., Szalaty, T. J., Szatkowski, T., and Jesionowski, T. (2016). "Lignosulfonate as a byproduct of wood pulp production: A potential precursor for the preparation of functional hybrid materials," *Ann. Univ. Mariae Curie-Sklodowska, Sect. AA–Chem.* 71(1), 47-68. https://doi.org/10.17951/aa.2016.71.1.47

Korbag, I., and Mohamed Saleh, S. (2016). "Studies on the formation of intermolecular interactions and structural characterization of polyvinyl alcohol/lignin film," *Int. J. Environ. Stud.* 73(2), 226-235. https://doi.org/10.1080/00207233.2016.1143700

Korbag, I., Eghreibeel, H., Mhmood, M. A., and Saleh, S. M. (2018). "Thermal properties of poly (vinyl alcohol) / lignin blends," *Al-Mukhtar J. Sci.* 33(4), 273-280. https://doi.org/10.54172/mjsc.v33i4.310

Kropat, M., Liao, M., Park, H., Salem, K. S., Johnson, S., and Argyropoulos, D. S. (2021). "A perspective of lignin processing and utilization technologies for composites and plastics with emphasis on technical and market trends," *BioResources* 16(1), 2084-2115. https://doi.org/10.15376/biores.16.1.KROPAT

Kubo, S., and Kadla, J. F. (2003). "The formation of strong intermolecular interactions in immiscible blends of poly(vinyl alcohol) (PVOH) and lignin," *Biomacromolecules* 4(3), 561-567.

Li, N., An, X., Xiao, X., An, W., and Zhang, Q. (2022). "Recent advances in the treatment of lignin in papermaking wastewater," *World J. Microbiol. Biotechnol.* 38(7), article 116. https://doi.org/10.1007/s11274-022-03300-w

Lin, J., Peng, Z., Liu, Y., Ruiz-Zepeda, F., Ye, R., Samuel, E. L. G., Yacaman, M. J., and Tour, J. M. (2014). "Laser-induced porous graphene films from commercial polymers," *Nat. Commun.* 5(5714), 1-8. https://doi.org/10.1038/ncomms6714

Luo, H., and Abu-Omar, M. M. (2017). "Chemicals from lignin," *Encycl. Sustain. Technol.* 3, 573-585. https://doi.org/10.1016/b978-0-12-409548-9.10235-0

Mudgil, D., Barak, S., and Khatkar, B. S. (2012). "X-ray diffraction, IR spectroscopy and thermal characterization of partially hydrolyzed guar gum," *Int. J. Biol. Macromol.* 50(4), 1035-1039. https://doi.org/10.1016/j.ijbiomac.2012.02.031

Nair, S. S., Sharma, S. K., Pu, Y., Sun, Q., Pan, S., Zhu, J. Y., Deng, Y., and Ragauskas, A. J. (2014). "High shear homogenization of lignin to nanolignin and thermal stability of nanolignin-polyvinyl alcohol blends," *ChemSusChem* 7 (12), 3513-3520. https://doi.org/10.1002/cssc.201402314

Nasef, S. M., Sayed, A., and Mahmoud, G. A. (2024). "Comparative study of lignin and sodium lignosulfonate extracted from irradiated and non-irradiated sawdust wastes," *Radiat. Phys. Chem.* 214, article 111302. https://doi.org/10.1016/j.radphyschem.2023.111302

Nouh, S. A., Alhazime, A. A., Benthami, K., Mahrous, E. M., and Barakat, M. M. (2023). "Structural and optical studies of gamma-irradiated polyvinyl alcohol, polyethylene glycol, and lignosulfonate thin film," *Radiat. Eff. Defects Solids* 178(1-2), 5-19. https://doi.org/10.1080/10420150.2023.2186865

Onyari, J. M., Mulaa, F., Muia, J., and Shiundu, P. (2008). "Biodegradability of poly (lactic acid), preparation and characterization of PLA/gum arabic blends," *J. Polym. Environ.* 16(3), 205-212. https://doi.org/10.1007/s10924-008-0096-5

Ou, J., and Zhao, J. (2017). "Modification of sodium lignosulfonate and evaluation of its potential use as detergent builders," *J. Wood Chem. Technol.* 37(2), 99-109. https://doi.org/10.1080/02773813.2016.1235589

Patel, S., and Goyal, A. (2015). "Applications of natural polymer gum arabic: A review," *Int. J. Food Prop.* 18(5), 986-998. https://doi.org/10.1080/10942912.2013.809541

Pereira, S. S., Faria, L. B., da Costa, J. P., Paiva, N., Martins, J., Carvalho, L. H., and Magalhães, F. D. (2021). "Lignosulfonates as an alternative to non-renewable binders in wood-based materials," *Polymers* 13(23), article 4196. https://doi.org/10.3390/polym13234196

Phansamarng, P., Bacchus, A., Pour, F. H., Kongvarhodom, C., and Fatehi, P. (2024). "Cationic lignin incorporated polyvinyl alcohol films for packaging applications," *Ind. Crops Prod.* 221, article 119217. https://doi.org/10.1016/j.indcrop.2024.119217

Rahman, S., Konwar, A., Majumdar, G., and Chowdhury, D. (2021). "Guar gum-chitosan composite film as excellent material for packaging application," *Carbohydr. Polym. Technol. Appl.* 2, article 100158. https://doi.org/10.1016/j.carpta.2021.100158

Raj, V., and Bajpai, A. (2020). "Synthesis of hydrophobically modified guar gum film for packaging materials," *Mater. Today Proc.* 29, 1132-1142. https://doi.org/10.1016/j.matpr.2020.05.339

Ramadhan, M. H., Nurrahman, A., Steven, S., and Mardiyati, Y. (2024). "Enhancing mechanical properties, degradation rate, and water resistance of bioplastic lignin/ polyvinyl alcohol (PVOH) by fractionation of lignin," *Emerg. Mater.* 8, 2231-2240. https://doi.org/10.1007/s42247-024-00805-y

Rawooth, M., Habibullah, S. K., Qureshi, D., Bharti, D., Pal, A., Mohanty, B., Jarzębski, M., Smułek, W., and Pal, K. (2022). "Effect of tamarind gum on the properties of phase-separated poly (vinyl alcohol) films," *Polymers* 14(14), article 2793. https://doi.org/10.3390/polym14142793

Rostamabadi, H., Demirkesen, I., Colussi, R., Roy, S., Tabassum, N., de Oliveira Filho, J. G., Bist, Y., Kumar, Y., Nowacka, M., Galus, S., *et al.* (2024). "Recent trends in the application of films and coatings based on starch, cellulose, chitin, chitosan, xanthan, gellan, pullulan, arabic gum, alginate, pectin, and carrageenan in food packaging," *Food Front.* 5(2), 350-391. https://doi.org/10.1002/fft2.342

Shaikh, H. M., Anis, A., Poulose, A. M., Madhar, N. A., and Al-Zahrani, S. M. (2022). "Date-palm-derived cellulose nanocrystals as reinforcing agents for poly (vinyl alcohol)/guar-gum-based phase-separated composite films," *Nanomaterials* 12(7), article 1104. https://doi.org/10.3390/nano12071104

Singh, K., Yuvrajsinh, G. M., Mehra, S., Mishra, A., and Kumar, A. (2024). "Bioionic liquid-assisted transparent sodium alginate-κ-carrageenan-lignin composite films with

excellent ultraviolet shielding, antioxidant, and antibacterial properties," *ACS Sustain. Chem. Eng.* 12(10), 4314-4327. https://doi.org/10.1021/acssuschemeng.4c00087

Su, S., and Fang, G. (2014). "Fabrication and properties of alkaline lignin/poly (vinyl alcohol) blend membranes," *BioResources* 8(2), 2510-2520. https://doi.org/10.15376/biores.8.2.2510-2520

TAPPI T211 om-02 (2002). "Ash in wood, pulp, paper, and paperboard: Combustion at 525ºC," TAPPI Press, Atlanta, GA, USA.

TAPPI T222 om-11. (2011). "Acid-insoluble lignin in wood and pulp," TAPPI Press, Atlanta, GA, USA.

Thombare, N., Mahto, A., Singh, D., Chowdhury, A. R., and Ansari, M. F. (2023). "Comparative FTIR characterization of various natural gums: A criterion for their identification," *J. Polym. Environ.* 31, 3372-3380. https://doi.org/10.1007/s10924-023-02821-1

Tian, R., Liu, Y., Wang, C., Jiang, W., Janaswamy, S., Yang, G., Ji, X., and Lyu, G. (2024). "Strong, UV-blocking, and hydrophobic PVOH composite films containing tunable lignin nanoparticles," *Ind. Crops Prod.* 208, article 117842.

Vigneshwaran, N., Ammayappan, L., and Huang, Q. (2011). "Effect of gum arabic on distribution behavior of nanocellulose fillers in starch film," *Appl. Nanosci.* 1(3), 137-142. https://doi.org/10.1007/S13204-011-0020-5

Wang, X., Zhu, Y., Wang, X., Liu, G., Li, J., Zhao, R., Zhang, Y., Zhang, X., Han, G., Zhao, H., *et al.* (2020). "*In-situ* growth of graphene on carbon nanofiber from lignin," *Carbon* 169, 446-454. https://doi.org/10.1016/j.carbon.2020.07.070

Wang, H., Liu, X., Wu, M., and Huang, Y. (2024). "Construction of multiple crosslinked networks for the preparation of high-performance lignin-containing cellulose nanofiber reinforced polyvinyl alcohol films," *Int. J. Biol. Macromol.* 259, article 129061. https://doi.org/10.1016/j.ijbiomac.2023.129061

Xia, Z., Akim, L. G., and Argyropoulos, D. S. (2001). "Quantitative 13C NMR analysis of lignins with internal standards," *J. Agric. Food Chem.* 49(8), 3573-3578. https://doi.org/10.1021/JF010333V

Xu, G., Ren, S., Wang, D., Su, L., and Fang, G. (2013). "Fabrication and properties of alkaline lignin/poly (vinyl alcohol) blend membranes," *BioResources* 8(2), 2510-2520. https://doi.org/10.15376/biores.8.2.2510-2520

Xu, Y. H., Li, M. F., and Peng, F. (2023). "Lignin micro/nanoparticles: Synthesis, properties, and application to endow polyvinyl alcohol film with multi-functionality," *Chem. Eng. J.* 473, article 145233. https://doi.org/10.1016/j.cej.2023.145233

Yang, H., Yuan, J., Chai, M., Sun, Z., Li, C., Meng, X., and Yao, L. (2024). "Excellent facile fabrication of PVA and lignin nanoparticles from wheat straw after novel DES-THF pretreatment," *Int. J. Biol. Macromol.* 281, article ID 136238. https://doi.org/10.1016/j.ijbiomac.2024.136238

Yang, L., Wang, D., Zhou, D., Zhang, Y., and Yang, T. (2017). "Isolation and further structural characterization of lignins from the valonea of *Quercus variabilis*," *Int. J. Biol. Macromol.* 97, 164-172. https://doi.org/10.1016/j.ijbiomac.2017.01.008

Ye, D. Z., Jiang, L., Hu, X. Q., Zhang, M. H., and Zhang, X. (2016). "Lignosulfonate as reinforcement in polyvinyl alcohol film: Mechanical properties and interaction analysis," *Int. J. Biol. Macromol.* 83, 209-215. https://doi.org/10.1016/j.ijbiomac.2015.11.064

Ysulat, M. L. M., Ysulat, J. A. N., Caparanga, A. R., Pasag, J. M., and Cruz, R. A. T. (2023). "Fabrication and surface characterization of lignin-polyamide thin film

composite membrane for reverse osmosis desalination," *J. Membr. Sci. Res.* 9(4), 481-487. https://doi.org/10.22079/jmsr.2023.1998807.1597

Zhang, X., Liu, W., Liu, W., and Qiu, X. (2020). "High performance PVOH/lignin nanocomposite films with excellent water vapor barrier and UV-shielding properties," *Int. J. Biol. Macromol.* 142, 551-558. https://doi.org/10.1016/j.ijbiomac.2019.09.129

Zhou, Q., Chen, J., Wang, C., Yang, G., Janaswamy, S., Xu, F., and Liu, Z. (2022). "Preparation and characterization of lignin nanoparticles and chitin nanofibers reinforced PVOH films with UV shielding properties," *Ind. Crops Prod.* 188, article 115669. https://doi.org/10.1016/j.indcrop.2022.115669

Article submitted: September 5, 2025; Peer review completed: November 1, 2025; Revised version received: January 13, 2026; Accepted: February 20, 2026; Published: March 2, 2026.
DOI: 10.15376/biores.21.2.3688-3717

APPENDIX

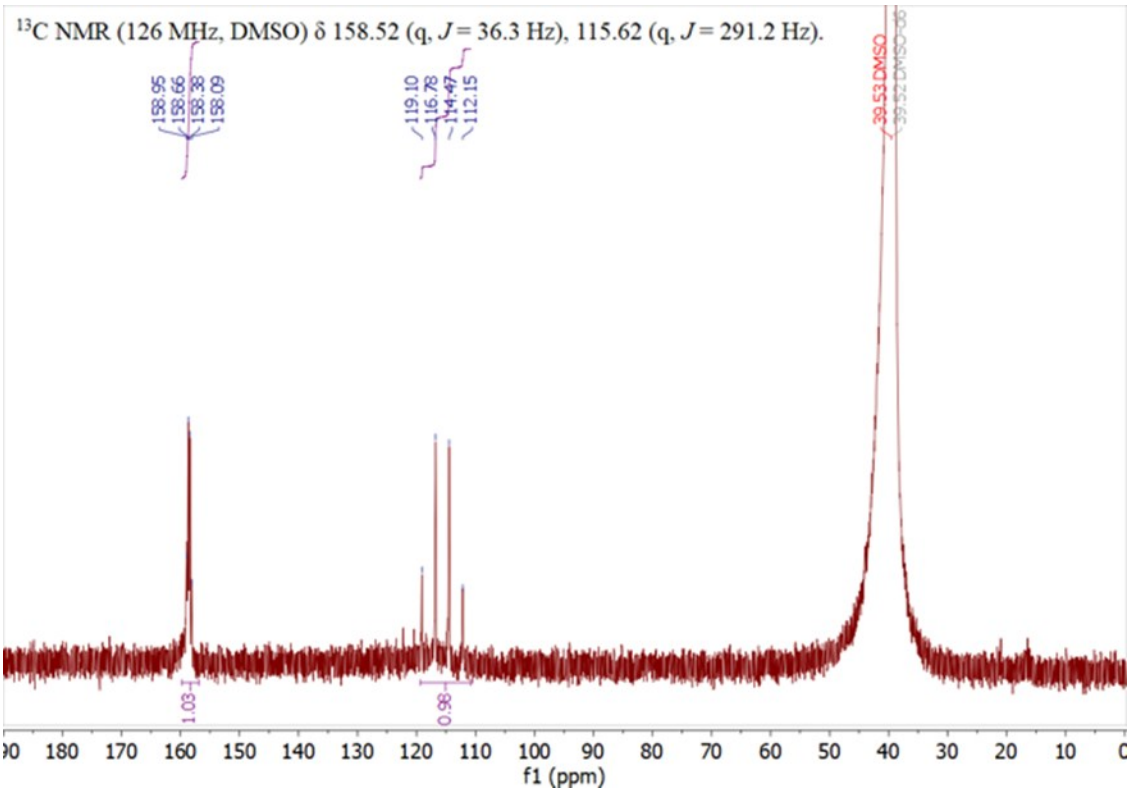

Fig. S1. ^{13}C-NMR spectrum obtained for neat LS

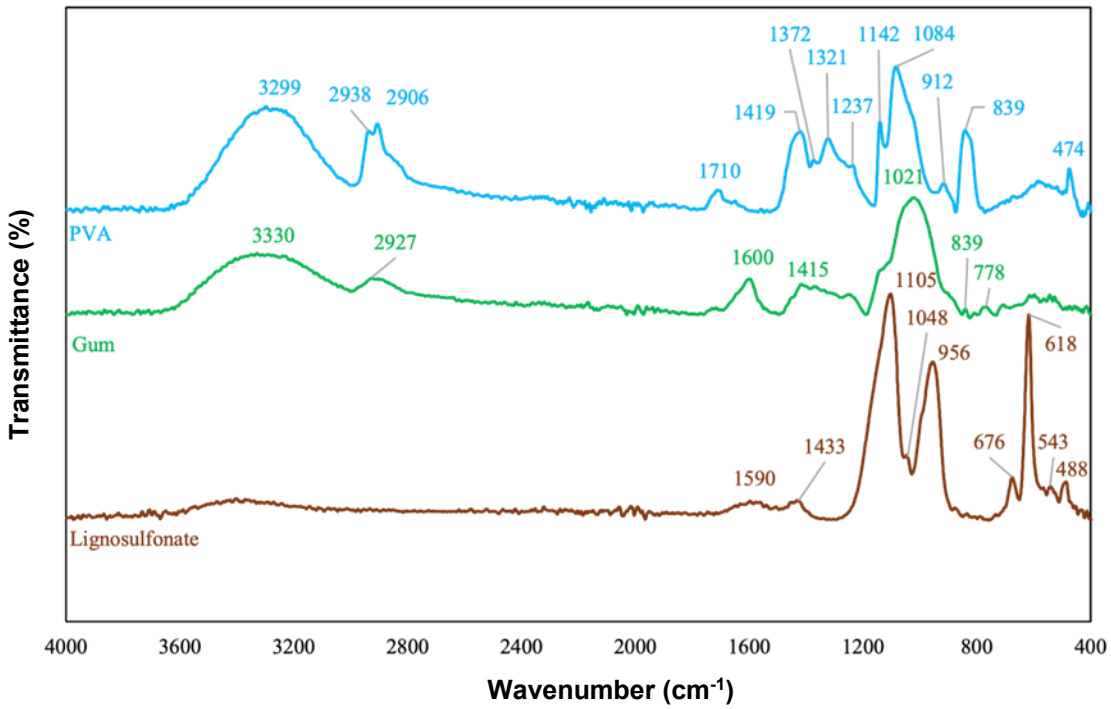

Fig. S2. FTIR spectra of neat polymers used in film production

Table S1. Average Mineral Contents of the Films After the Mapping Process Performed on SEM Images (60 min Pre-evaporation and 0 to 25% GA Addition)

	C	O	Na	S
0% Bottom	26.90	34.75	32.80	5.55
0% Top	26.45	22.45	51.10	0.00
1% Bottom	25.60	42.20	21.80	10.40
1% Top	27.20	36.95	26.40	9.45
5% Bottom	29.45	48.65	17.50	4.40
5% Top	24.30	42.40	19.40	13.90
10% Bottom	22.50	34.40	31.60	11.50
10% Top	32.90	42.65	18.45	6.00
25% Bottom	24.65	44.95	20.05	10.35
25% Top	31.15	37.65	12.45	18.75

Table S2. Average Mineral Contents of the Films After the Mapping Process Performed on SEM Images (90 min Pre-evaporation and 0 to 25% GA Addition)

	C	O	Na	S
0% Bottom	19.80	42.30	20.30	17.60
0% Top	29.97	34.20	25.80	10.03
1% Bottom	25.25	40.60	24.90	9.25
1% Top	21.00	32.23	32.73	14.03
5% Bottom	34.00	46.80	16.95	2.25
5% Top	33.35	45.30	16.55	4.80
10% Bottom	22.90	40.60	26.80	9.70
10% Top	26.57	43.30	25.17	4.97
25% Bottom	30.57	33.33	33.97	2.13
25% Top	28.50	43.10	19.55	8.85

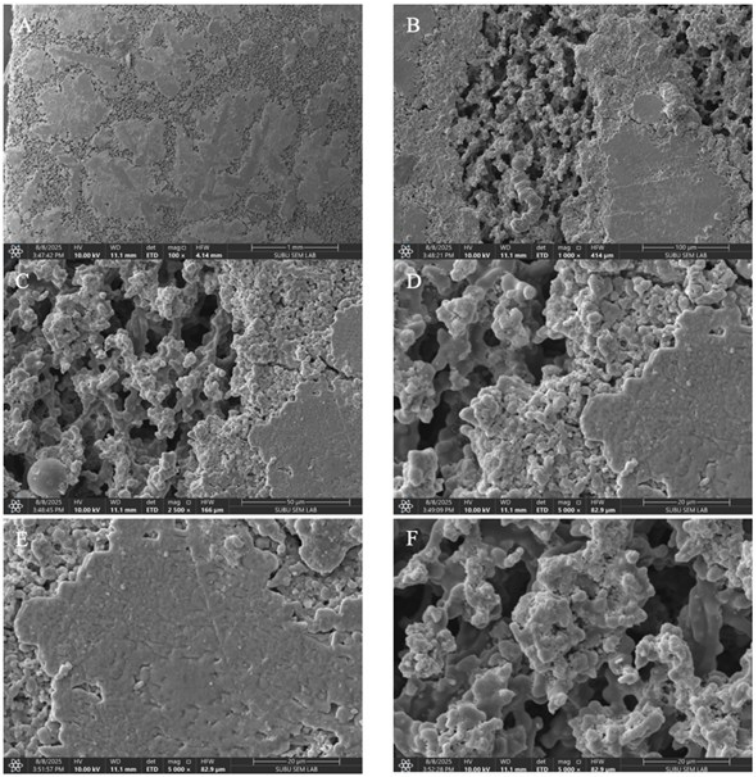

Fig. S3. Electron microscope images of the bottom surface of the film without gum addition for 60 min (A: 100x, B: 1000x, C: 2500x, D: 5000xa, E: 5000xb and F: 5000xc)

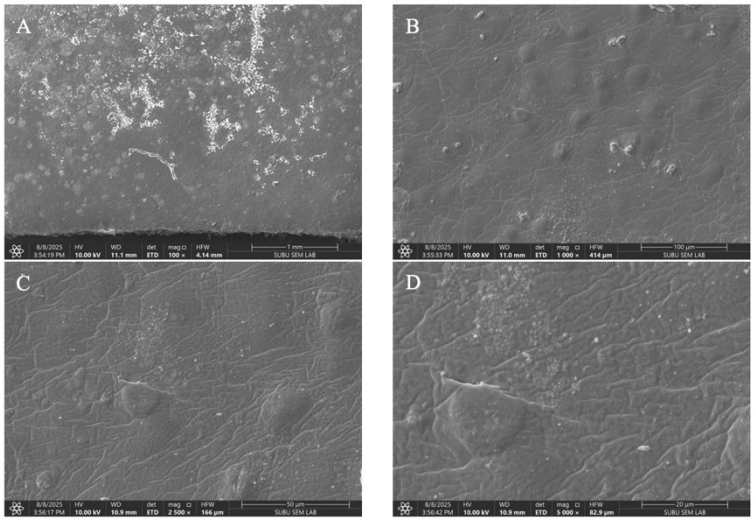

Fig. S4. Electron microscope images of the top surface of the film without gum addition for 60 min (A: 100x, B: 1000x, C: 2500x and D: 5000x)

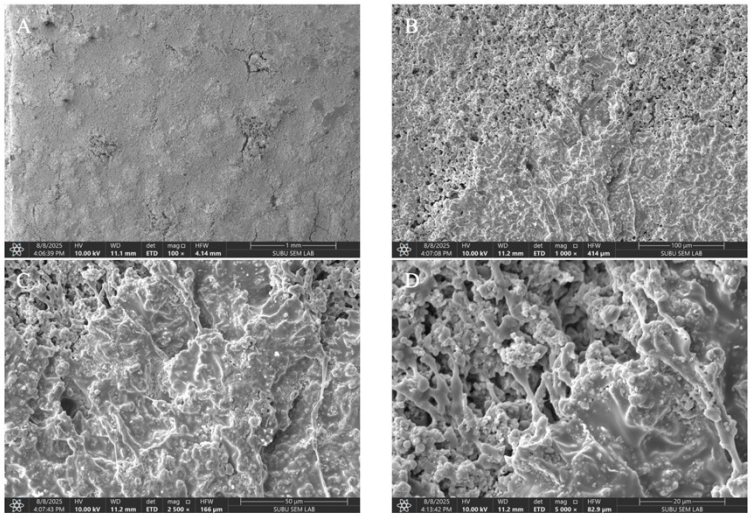

Fig. S5. Electron microscope images of the bottom surface of the film with 1% gum addition for 60 min (A: 100x, B: 1000x, C: 2500x, D: 5000xa, E: 5000xb, and F: 5000xc)

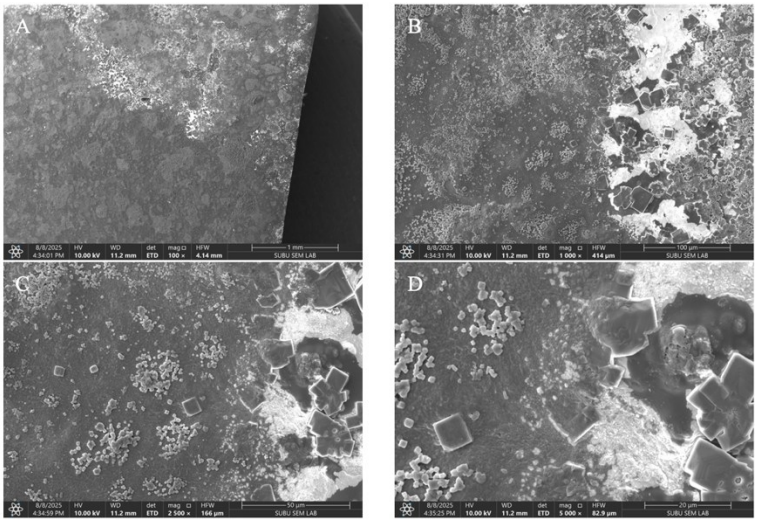

Fig. S6. Electron microscope images of the top surface of the film with 1% gum addition for 60 min (A: 100x, B: 1000x, C: 2500x and D: 5000x)

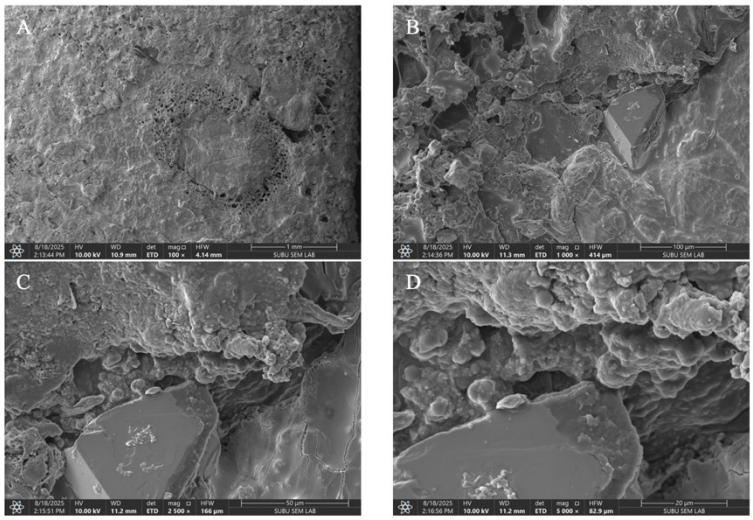

Fig. S7. Electron microscope images of the bottom surface of the film with 5% gum addition for 60 min (A: 100x, B: 1000x, C: 2500x, D: 5000xa, E: 5000xb and F: 5000xc)

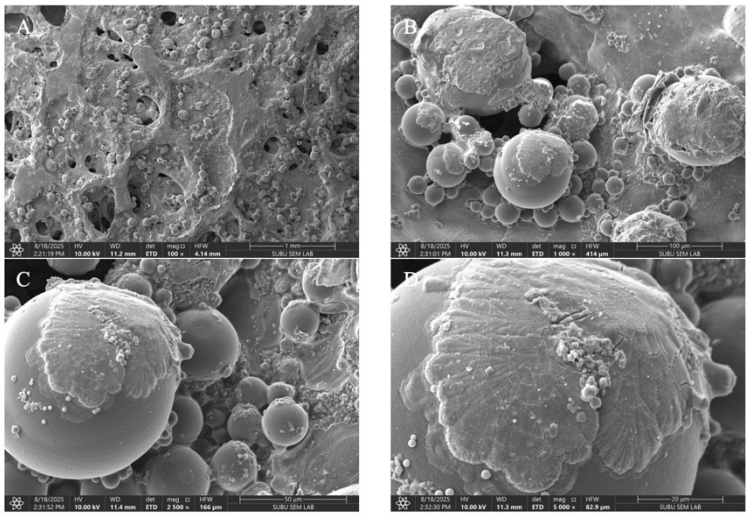

Fig. S8. Electron microscope images of the top surface of the film with 5% gum addition for 60 min (A: 100x, B: 1000x, C: 2500x and D: 5000x)

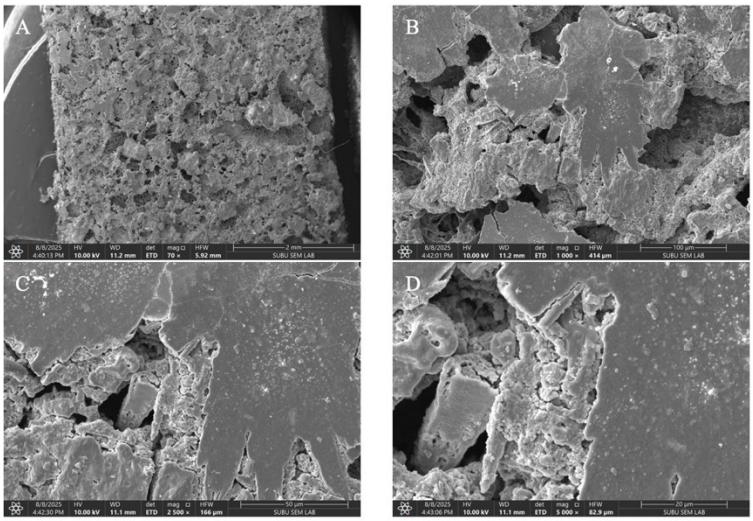

Fig. S9. Electron microscope images of the bottom surface of the film with 5% gum addition for 60 min (A: 100x, B: 1000x, C: 2500x, D: 5000xa, E: 5000xb and F: 5000xc)

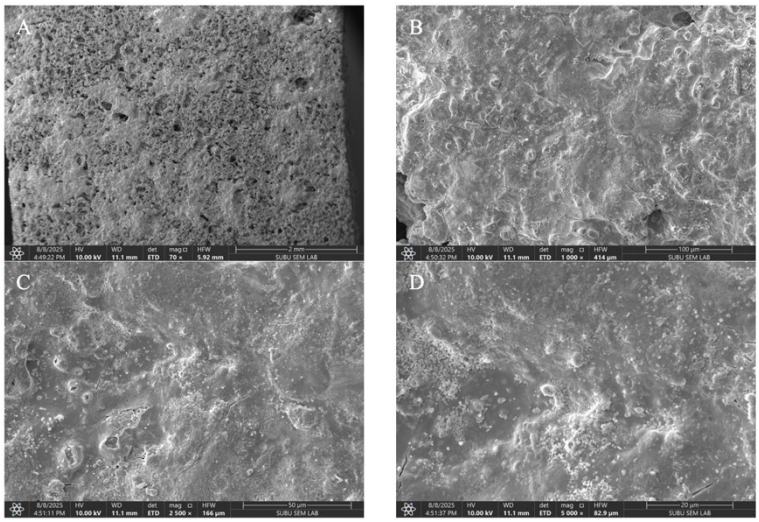

Fig. S10. Electron microscope images of the top surface of the film with 10% gum addition for 60 min (A: 100x, B: 1000x, C: 2500x and D: 5000x)

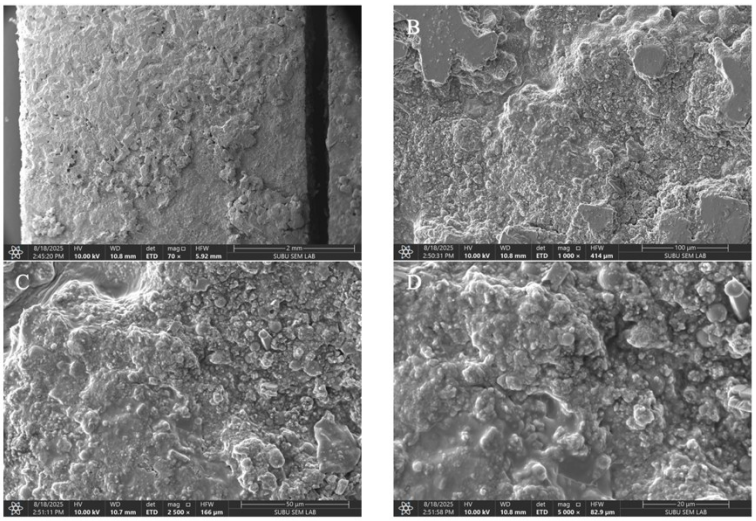

Fig. S11. Electron microscope images of the bottom surface of the film with 25% gum addition for 60 min (A: 100x, B: 1000x, C: 2500x, D: 5000xa, E: 5000xb and F: 5000xc)

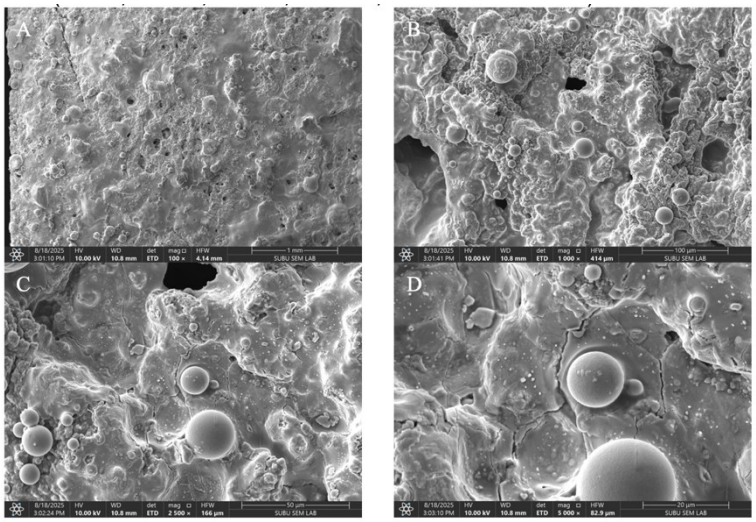

Fig. S12. Electron microscope images of the top surface of the film with 25% gum addition for 60 min (A: 100x, B: 1000x, C: 2500x and D: 5000x)

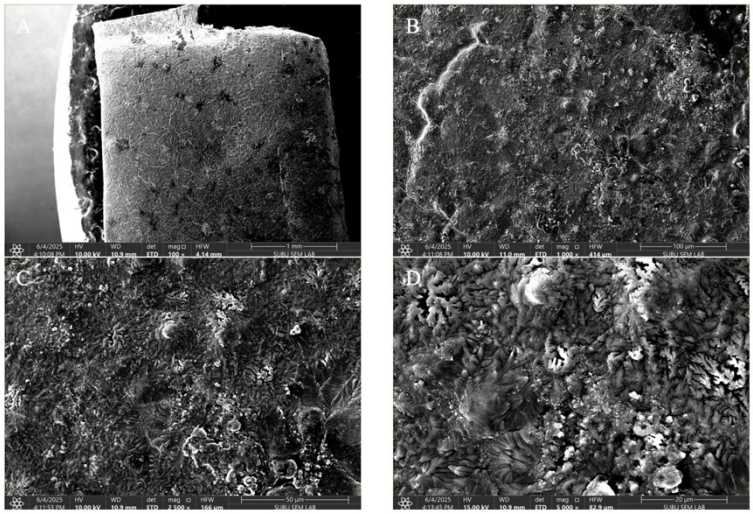

Fig. S13. Electron microscope images of the bottom surface of the film without gum addition for 90 min (A: 100x, B: 1000x, C: 2500x, D: 5000xa, E: 5000xb and F: 5000xc)

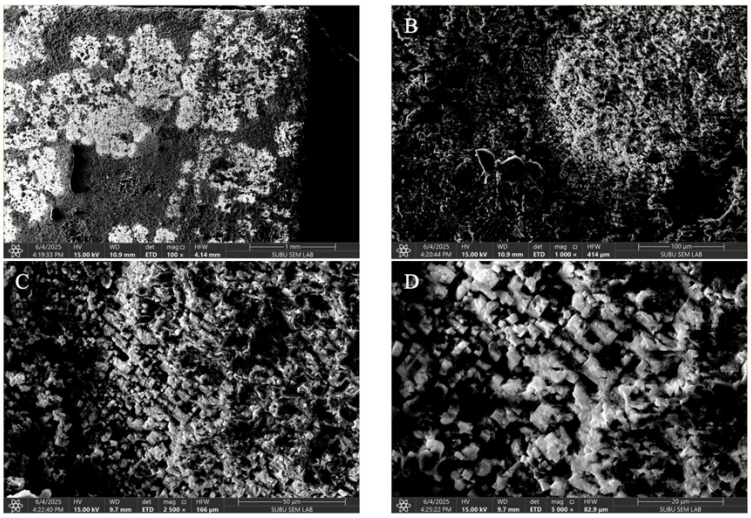

Fig. S14. Electron microscope images of the top surface of the film without gum addition for 90 min (A: 100x, B: 1000x, C: 2500x and D: 5000x)

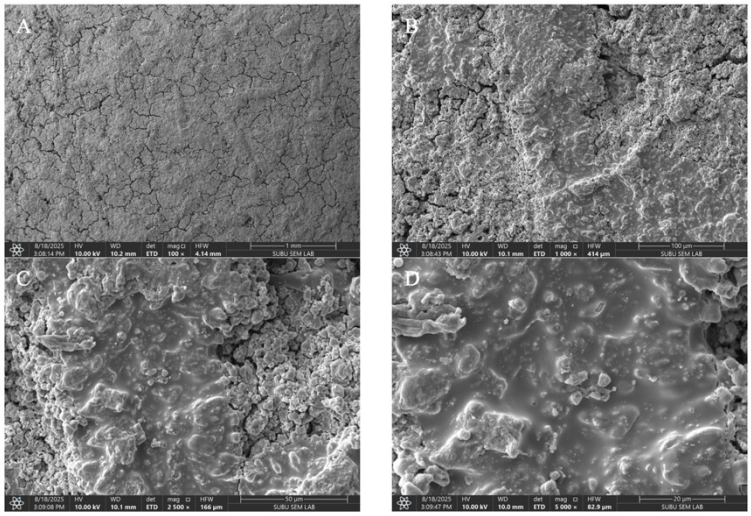

Fig. S15. Electron microscope images of the bottom surface of the film with 1% gum addition for 90 min (A: 100x, B: 1000x, C: 2500x, D: 5000xa, E: 5000xb and F: 5000xc)

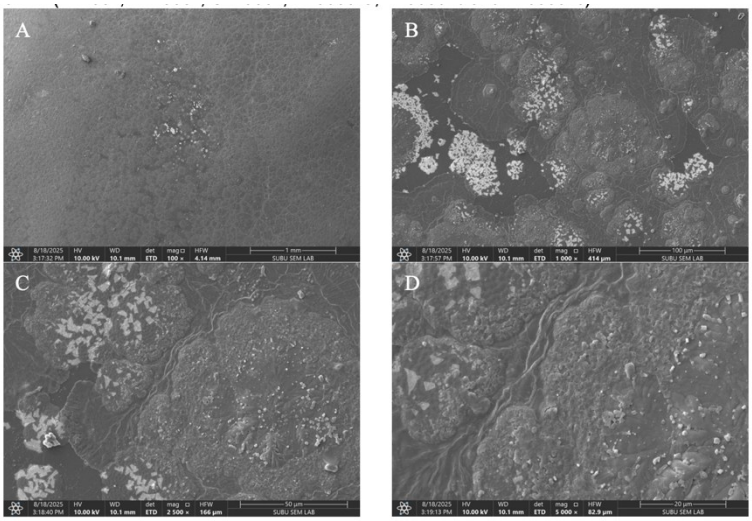

Fig. S16. Electron microscope images of the top surface of the film with 1% gum addition for 90 min (A: 100x, B: 1000x, C: 2500x and D: 5000x)

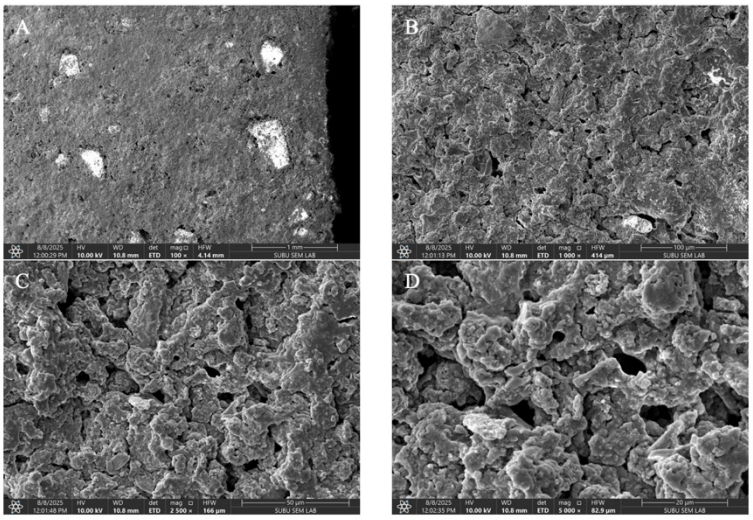

Fig. S17. Electron microscope images of the bottom surface of the film with 5% gum addition for 90 min (A: 100x, B: 1000x, C: 2500x, D: 5000xa, E: 5000xb and F: 5000xc)

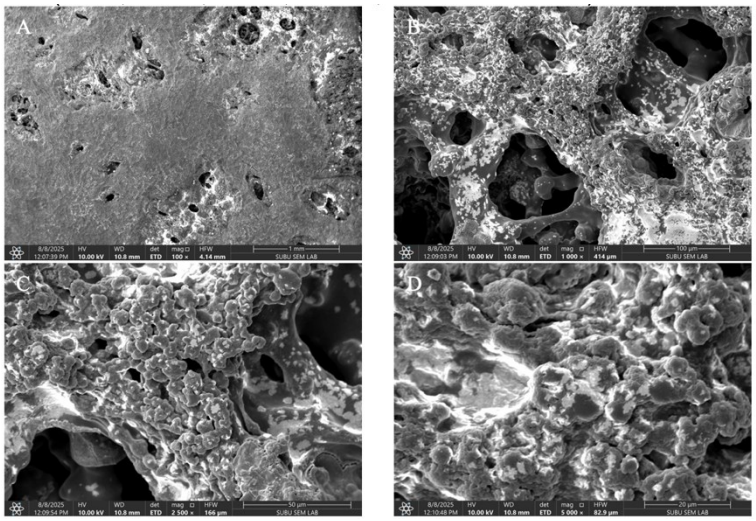

Fig. S18. Electron microscope images of the top surface of the film with 5% gum addition for 90 min (A: 100x, B: 1000x, C: 2500x and D: 5000x)

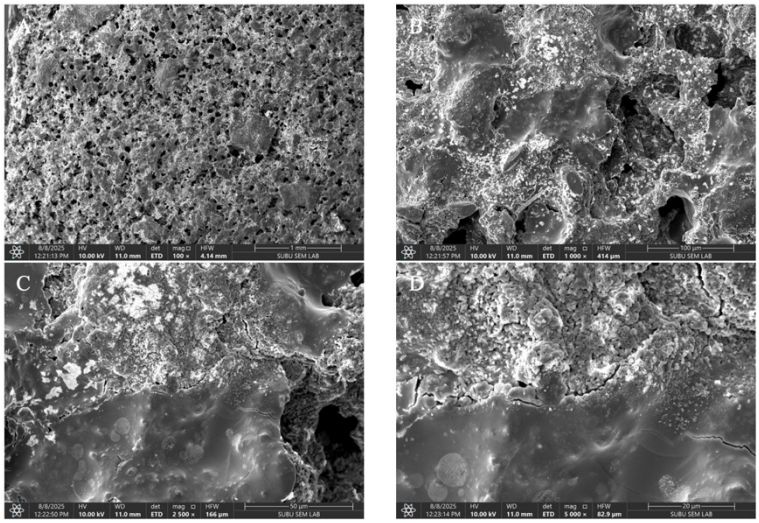

Fig. S19. Electron microscope images of the bottom surface of the film with 10% gum addition for 90 min (A: 100x, B: 1000x, C: 2500x, D: 5000xa, E: 5000xb and F: 5000xc)

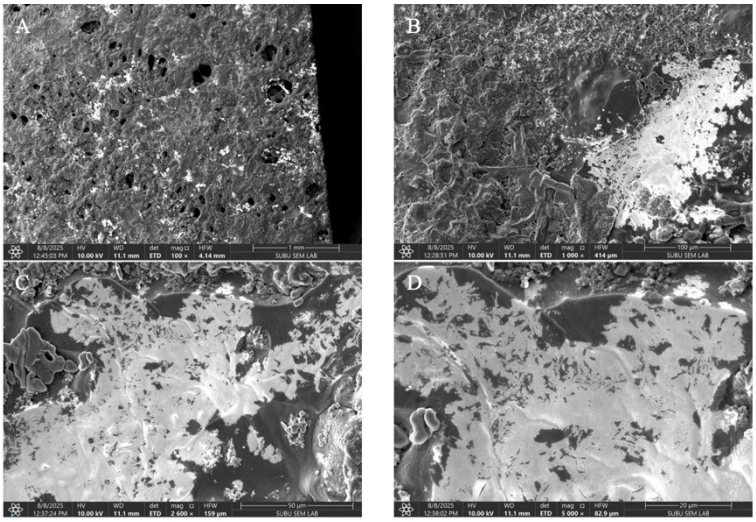

Fig. S20. Electron microscope images of the top surface of the film with 10% gum addition for 90 min (A: 100x, B: 1000x, C: 2500x and D: 5000x)

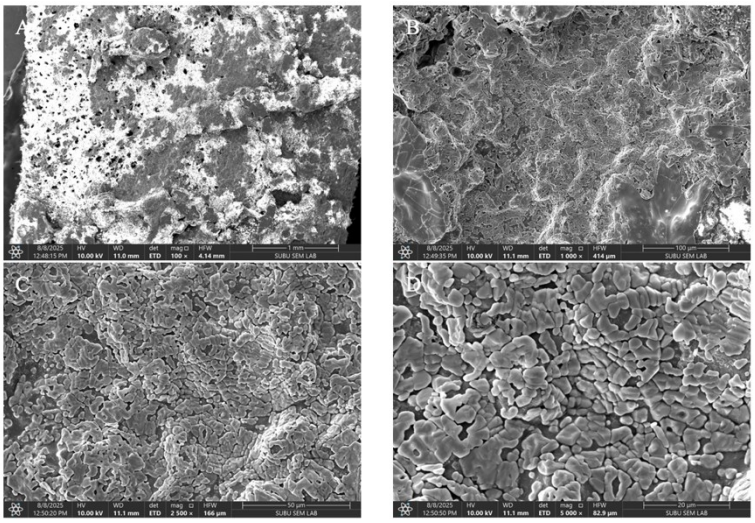

Fig. S21. Electron microscope images of the bottom surface of the film with 25% gum addition for 90 min (A: 100x, B: 1000x, C: 2500x, D: 5000xa, E: 5000xb and F: 5000xc)

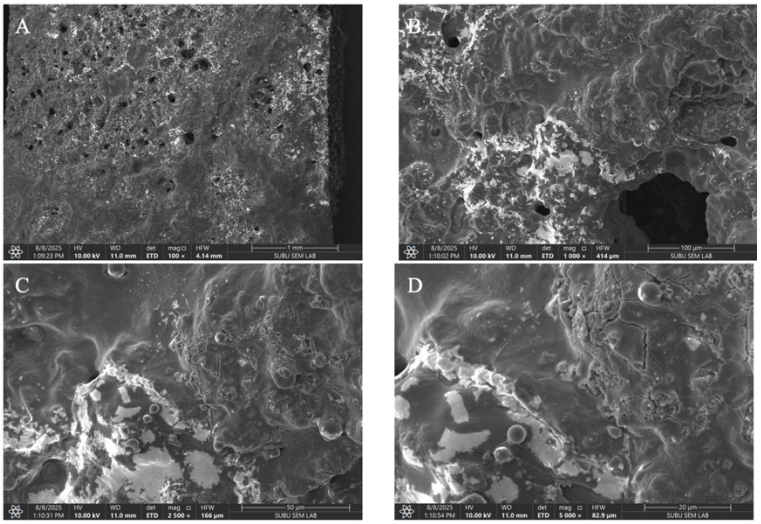

Fig. S22. Electron microscope images of the top surface of the film with 25% gum addition for 90 min (A: 100x, B: 1000x, C: 2500x and D: 5000x)